Analytical Evaluation of Surface-Mounted PMSG Performances Connected to a Diode Rectifier

M. F. Iacchetti, *Member, IEEE*, G. M. Foglia, A. Di Gerlando, *Member, IEEE* ,
A. J. Forsyth, *Senior Member, IEEE*

***Abstract*—This paper analyzes some operational issues of three-phase surface-mounted permanent magnet synchronous generators connected to a diode rectifier. This simple configuration coupled to a single-switch dc-dc converter is used in small scale wind energy conversion systems as well as in energy harvesting systems, to reduce costs. The diode rectifier causes an intrinsic limit for the maximum convertible power which is related to the load impedance matching, and additional joule losses due to the distorted currents. By using an analytical steady-state model of the rectifier and of the PMSG, this paper discusses how to achieve two particularly meaningful operating conditions characterized respectively by the maximum power transfer and the maximum power per ampere. The theory is validated by simulation and test results on a prototype.**

***Index Terms*—surface mounted PMSMs, rectifier, fractional-slot windings, PMSG design.**

NOMENCLATURE

E_{pk}	peak value of the phase EMF
I_0 , I_{rms}	average dc, rms ac current
k_R	resistance increase coefficient due to the eddy currents
m	ratio V_{dc}/E_{pk}
p	pole number
L, R	synchronous inductance, resistance
R_D	diode incremental resistance
V_{dc}	dc-bus voltage
V_D	threshold voltage drop across the diode
Z	equivalent stator impedance, including R_D
η	efficiency of the PMSG + diode rectifier
φ_Z	characteristic angle of the impedance Z
ω, ω_m	stator angular frequency, mechanical speed (rad/s)

Superscripts

*	p.u. value in the basis { E_{pk} , Z }

Subscripts

0	dc side
n	rated value

Manuscript received August 1, 2014; revised February 9, 2015; accepted June 5, 2015.

M. F. Iacchetti and A. J. Forsyth are with the School of Electrical and Electronic Engineering of the University of Manchester, Sackville Street Building, Sackville Street, M1 3BB Manchester (UK), e-mail: [matteo.iacchetti, Andrew.Forsyth]@manchester.ac.uk.

G. M. Foglia and A. Di Gerlando are with the Dipartimento di Energia, Politecnico di Milano, piazza L. Da Vinci 32, 20133 Milano, e-mail: [gianmaria.foglia, antonino.digerlando]@polimi.it.

I. INTRODUCTION

PERMANENT MAGNET synchronous generators (PMSGs) are widely used in renewable power generation due to the high efficiency and power density [1]-[2]. They can be effectively controlled by a PWM converter acting as a controlled rectifier. This way, the *d*-axis and *q*-axis currents can be independently regulated, allowing at the same time the control of the prime mover around the maximum power point, and the implementation of the maximum torque per ampere control [3] or minimum global loss control [4].

Mainly in order to reduce the costs, the inverter can be replaced by a full bridge diode rectifier followed by a dc-dc single-switch converter [5]-[7]. Further conversion solutions have also been proposed in order to mitigate the detrimental effects due to the harmonics [8] and to achieve a trade-off between the costs and the regulation capability. For instance: multi-pulse rectifying schemes [9], thyristor-connected diode bridges for a variable parallel to series connection [10], switchable-cascaded-mode boost chopper based on diode bridges and single-switch boost converters [11], semi-controlled PWM rectifiers [12].

When the PMSG is controlled by a PWM rectifier, the maximum achievable power is essentially limited by the constraints related to the insulation and to the cooling, whereas the PMSG inductance and the electromotive force (EMF) affect the converter size [13]. By contrast, a PMSG connected to a diode rectifier exhibits an intrinsic limit of the maximum convertible power, that depends on the internal impedance of the generator [14], according to the load matching impedance concept. Moreover the existence of an operating condition which maximizes the ratio dc power to ac rms current can be suspected. The knowledge of the maximum power (MP) and maximum power per ampere (MPPA) operating conditions as a function of the machine parameters would be useful for an optimized design of the PMSG.

The dc-dc converter placed after the diode rectifier makes available only one degree of freedom for the control of the system: namely, the voltage across the diode bridge. This is usually adjusted in order to optimize the operation of the prime mover in such a way as to extract the maximum allowable power [5], [7]. However, there are also some situations where

the regulation of the prime mover is totally independent from the control of the PMSG. Typically, this happens when a small PMSG is coupled to a large prime mover to feed ancillary systems, as in automotive [14]-[15] or aircraft applications [16]-[17]. In such a situation, the dc voltage can be controlled in order to optimize the operation of the PMSG at a given speed, imposed by the prime mover. To this purpose, the dc voltage which produces the MP or the MPPA operation should be initially identified as a function of the speed, yielding the MP or the MPPA trajectories.

Few works in the literature concern this topic, due to the difficulty in modeling the behavior of the diode rectifier in a closed form. Average models [18]-[19] are mainly suitable for the dynamical analysis. The behavior of diode bridge feeding dc active source was traditionally assessed by experiments and simulations [20],[21]. Steady-state analytical models of the three-phase diode rectifier with constant dc voltage or capacitive dc-bus have been developed only in recent years. The early steady-state models only deal with the operation in continuous conduction mode [22]-[23]. They are mainly devoted to the analysis of Lundell alternators, which are characterized by a high synchronous reactance, so that the rectifier operates in continuous conduction mode (CCM). By contrast, the lower inductance associated with the higher equivalent air-gap in PMSGs, results in the rectifier operating with discontinuous ac currents over a wide range: this operation mode is not covered at all by models [20] and [21]. Moreover, in small size PMSMs, the internal impedance cannot be approximated with a pure inductance and the model in [21] becomes inadequate. A model valid for all the operation modes and including the effect of the ac resistance has been developed in [24] and implicit analytical relations have been deduced in order to calculate the dc power and the efficiency in a three phase rectifier connected to a constant voltage source. In [24], only a partial discussion about how to obtain the maximum power transfer has been provided. The maximum power which can be transferred has not been evaluated, and the conditions for the MPPA have not been discussed at all. Moreover, the model in [24] has been experimentally validated only in case of ac reactors in series with an ac source, and not on a PMSG. Hidden dynamics for instance caused by the reaction of eddy currents in PMs or excited by higher harmonics in the EMF could introduce some deviation in the measurements on a PMSG with respect to the predictions of [24].

This paper provides an experimental validation of the model of the three-phase rectifier [24] in the case of connection to a PMSG. It also inquires into the MP and MPPA operation and deduces suitable analytic compact expressions for the required p.u. dc voltage in order to meet such conditions. These expressions help the designer to choose the most proper design parameters of a PMSG, thereby locating the rated operating point (for a given rated dc voltage) in the most desirable high-performance operation area. Additionally, in special cases where the prime mover is regulated independently of the PMSG, the presented theory also provides insight on how to schedule the dc voltage to optimize the performance of the PMSG + rectifier system.

The paper is organized as follows. Sec. II describes the considered system, and Section III resumes the behavior of a three-phase diode bridge rectifier connected to a constant voltage source and provides the analytical framework to evaluate the performance of a PMSG connected to the rectifier. The conditions to achieve the MP and the MPPA operation are deduced in Sec. III and IV, respectively. Section V provides some further remarks concerning the eddy current losses due to the skin effect in the windings. The most significant operating trajectories are discussed in Section VI. Finally, in section VII, the theory is validated by some simulation and experimental tests on a fractional slot, surface mounted PMSG.

II. Modeling of a Surface Mounted PMSG

The system considered in this paper is shown in Fig. 1 and consists of a three-phase PMSG coupled to a diode bridge rectifier connected to a constant dc voltage bus.

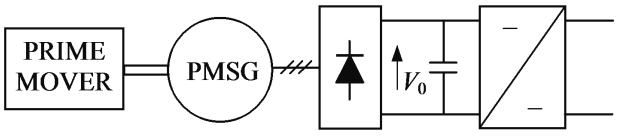

Fig. 1. Three-phase PMSG coupled to a diode bridge rectifier connected to a constant voltage dc bus.

The hypotheses of constant voltage is reasonable also when the rectifier is connected to a capacitive dc-bus either directly or through a dc-dc converter, whose switching frequency is sufficiently higher than the fundamental frequency of the EMF [14]. Fig. 2 shows the steady-state electrical model of the system: the PMSG is represented by its internal sinusoidal electromotive forces (EMFs) e_k (k=1,2,3) and by its internal resistance R and inductance L.

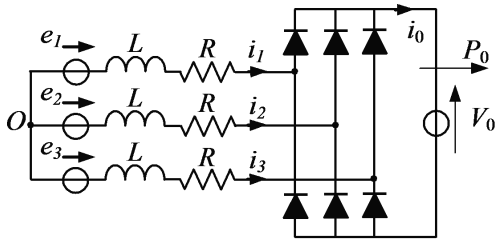

Fig. 2. Steady-state equivalent circuit of the system in Fig. 1.

The internal EMFs are expressed by

$$e_k(t) = E_{pk} \sin\left(\omega t - (k-1)\frac{2}{3}\pi\right) \tag{1}$$

The peak value E_{pk} of the internal EMF in (1) is

$$E_{pk} = \omega k_w N \varphi = k_E \omega \tag{2}$$

where k_w is the winding factor for the fundamental harmonic, N is the number of turns in series per phase, φ the pole flux (peak value) and ω is the stator angular frequency.

In order to evaluate the efficiency of the PMSG in the scheme

in Fig. 1, the iron losses are approximated by the no load iron losses and also mechanical losses are considered. The following expression is used

$$P_{fe,m} = \omega(c_0 + c_1\omega), \tag{3}$$

here c_0 lumps the frictional mechanical and hysteresis losses and c_1 mainly takes into account the eddy current losses.
The losses in the permanent magnets due to the space harmonics of the magneto motive force (MMF) as well as to the tooth-slot flux pulsations are not considered in this work; however, in small rating machines they have a minor effect.

III. Behavior of a Diode Rectifier with Constant DC Voltage

The theory developed in [24] shows that the behavior of the rectifier in Fig. 1 can be described in terms of the two parameters m and φ_Z:

$$m \equiv \frac{V_0 + 2V_D}{E_{pk}} \quad , \quad \cos\varphi_Z = \frac{R + R_D}{Z} \ , \tag{4}$$

where Z is the modulus of the internal impedance including the incremental resistance of the diodes

$$Z = \sqrt{(R+R_D)^2 + (\omega L)^2} \ . \tag{5}$$

In [24], it has been proven that the rectifier can work in four modes, namely: 2/0, 2/3/2/0, 2/3, and 3/3 (or CCM). The occurrence of each mode depends on the value of m. Voltage and current waveforms are shown in Fig. 3: mode 2/3/2/0 is not included, due to its very narrow region of existence in the plane (φ_Z , m). Also mode 2/0 will be disregarded, because, with PMSGs, it gives rise to a very low power transfer.

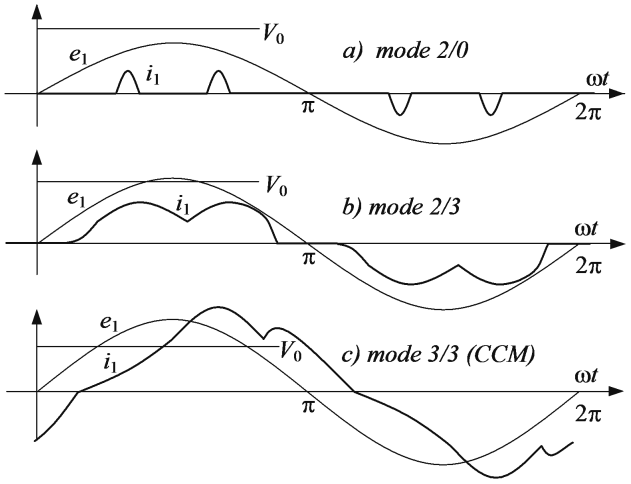

Fig. 3. Waveforms and operation modes 2/3 and 3/3 in the system of Fig. 2.

According to [24] the average dc current and the ac rms current can be expressed as

$$I_0 = \frac{E_{pk}}{Z} I_0^*(\theta_x, m, \varphi_Z), \tag{6}$$

$$I_{rms} = \frac{E_{pk}}{Z} I_{rms}^*(\theta_x, m, \varphi_Z). \tag{7}$$

In (6)-(7), the angle θ_x is an auxiliary variable which is associated to an additional constraint equation in the form

$$F(\theta_x, m, \varphi_Z) = 0 \ . \tag{8}$$

The system of two equations (6) or (7) and (8) implicitly defines I_0 or I_{rms} as a function of only the two variables m and φ_Z . The expressions of $I_0^*(\theta_x, m, \varphi_Z)$, $I_{rms}^*(\theta_x, m, \varphi_Z)$ and $F(\theta_x, m, \varphi_Z)$ are not reported here: they can be found in [24] for each operation mode in Fig. 3. Only for operation in CCM (mode 3/3), are explicit expressions available for I_0 and I_{rms} in terms of only m and φ_Z , avoiding the use of the additional variable θ_x and (8).
The power delivered to the dc bus P_0 is expressed as

$$P_0 = \frac{E_{pk}^2}{Z} P_0^*(\theta_x, m, \varphi_Z) \quad , \tag{9}$$

where

$$P_0^*(\theta_x, m, \varphi_Z) = \left(m - \frac{2V_D}{E_{pk}} \right) I_0^*(\theta_x, m, \varphi_Z). \tag{10}$$

If ideal diodes are assumed, the function $P_0^*(\theta_x, m, \varphi_Z)$ takes the compact form $P_0^*(\theta_x, m, \varphi_Z) = m \cdot I_0^*(\theta_x, m, \varphi_Z)$.
Again, it is worth to highlight that (8) must be considered appended to (6)-(7) or (10) in order to eliminate θ_x so that only the dependence on m and φ_Z survives.
Finally, by considering the operation of the rectifier coupled to a PMSG, the expression of the efficiency in [24] must be modified in order to incorporate at least the iron and mechanical losses lumped in $P_{fe,m}$ (3). The final expression is

$$\eta = \frac{P_0^*}{P_0^* + 3I_{rms}^{*2}\cos\phi_Z + 2I_0^* \frac{V_D}{E_{pk}} + P_{fe,m} \frac{Z}{E_{pk}^2}} \ . \tag{11}$$

Very meaningful operation charts providing the p.u. power P_0^* delivered to the dc-bus and the efficiency have been obtained in [24] for the particular case of ideal diodes (with V_D =0 and R_D =0) and with $P_{fe.m}$ = 0.In these conditions, only the first two terms in the denominator of (11) exist, so that, thanks to (10) (with V_D =0) and (8), η in (11) is a function of only m and φ_Z. Such operation charts are shown in Figs. 4 and 5: the blue lines represent the iso- P_0^* as well as the iso-η lines in the plane (φ_Z , m). These figures also show the boundaries (black bold lines) between the various operation modes of the system.

It is worth to notice that the model can also be extended to the parallel R-C load (instead of the constant voltage source), provided that the capacitance is large enough to limit the ripple in the DC voltage to a reasonable value (for instance 5-10%).
To this purpose, an equivalent DC voltage source which is a function of the dc load resistance is considered [24].

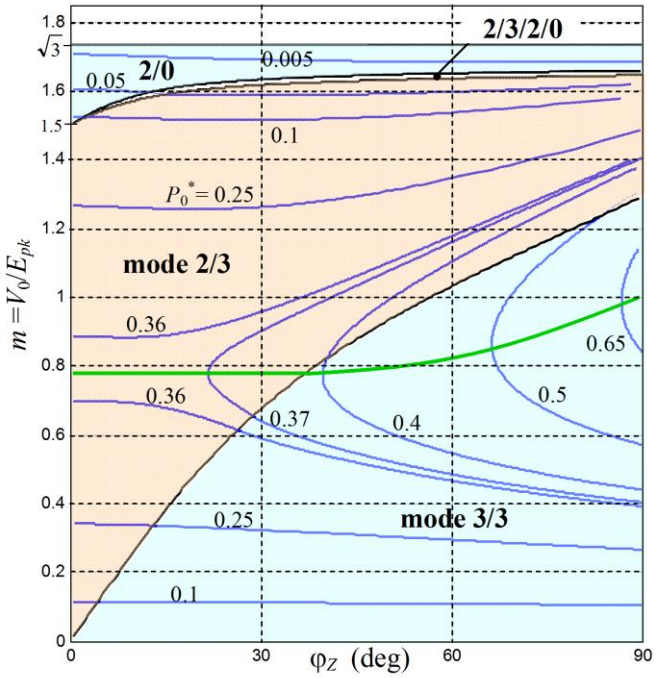

Fig. 4. Iso-P_0^* contour lines (blue), operation modes boundary lines (black) and locus of the maxima of P_0^* (green) in the plane (φ_Z , m)), for ideal diodes and for $P_{fe,m}$=0 (from [24]).

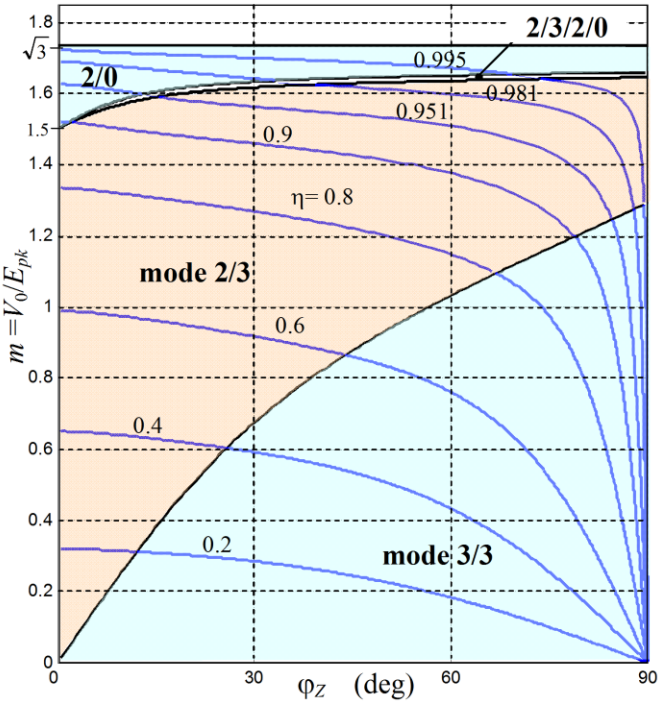

Fig. 5. Iso-η contour lines (blue), operation modes boundary lines (black) in the plane (φ_Z , m)), for ideal diodes and for $P_{fe,m}$=0 (from [24]).

IV. Maximum Power Operation

The green line in Fig.4 which connects the noses of the iso-P_0^* curves is the locus of the maxima of P_0^*: it provides the optimal value m_{MP} of m which maximizes P_0^* for a given φ_Z. An approximate expression of m_{MP} (φ_Z) suitable for practical evaluations has been deduced

$$m_{MP}(\varphi_Z) \cong \begin{cases} 0.78 & \text{if} \quad 0 < \varphi_Z \le 0.65 \text{ rad} \quad (\approx 37 \text{deg}) \\ 0.217\varphi_Z^2 - 0.229\varphi_Z + 0.837 & \text{otherwise} \end{cases} . \quad (12)$$

The corresponding values of P_0^* and I_{rms}^* which have not been provided in [24] are well approximated by

$$P_{0\,MP}^*(\varphi_Z) \cong 0.365 + 0.029\,\varphi_Z^2 + 0.06\varphi_Z^3 + 0.0025\varphi_Z^4 , \quad (13)$$

$$I_{rms\,MP}^*(\varphi_Z) \cong 0.364 + 0.011\varphi_Z^2 + 0.053\varphi_Z^3 - 0.015\varphi_Z^4 . \quad (14)$$

It should be remembered that, in order to obtain the actual (dimensional) power, (13) must be multiplied by E_{pk}^2/Z.

V. Maximum Power per Ampere Operation

A very interesting issue consists in studying the operating conditions which maximize the power transfer P_0 for a given ac rms current value I_{rms} , i.e. the MPPA condition. In fact, since the joule losses in the stator windings are generally predominant (except for very high speed machines), the MPPA points are very close to the maximum efficiency points. By solving (7) with respect to E_{pk}/Z and by replacing the result into (9), the power P_0 can be rewritten as

$$P_0 = E_{pk} I_{rms} \frac{P_0^*(\theta_x, m, \varphi_Z)}{I_{rms}^*(\theta_x, m, \varphi_Z)} . \quad (15)$$

From (15), the MPPA operation is achieved by maximizing the ratio

$$\xi = \frac{P_0^*(\theta_x, m, \varphi_Z)}{I_{rms}^*(\theta_x, m, \varphi_Z)} \quad (16)$$

with respect to the variable m . It must be remembered that the constraint equation (8) must be appended to (16), in order to eliminate the ancillary variable θ_x: this way, ξ becomes a function of only m and φ_Z . Moreover, the angle φ_Z plays the role of a parameter depending on the PMSG and on the speed, whereas m is a free control variable which can be adjusted by varying the dc voltage according to (4a).

Fig. 6 shows the iso - contour lines of (16) with V_D = 0 (ideal diodes) in the plane (φ_Z , m), i.e. considering any possible operation point of the diode bridge connected to a generic PMSG: they have been obtained by using the expressions of (6)-(8) and (10) given in [24].

The locus (red line) of the noses of the contour lines represents the MPPA operation points. Differently from the points (12) concerning the maximum power transfer (see Fig. 4), the MPPA points always belong to the region of mode 2/3 and the operation is also relatively far from mode 3/3. This confirms that the operation in mode 2/3 is the most interesting to achieve good performances.

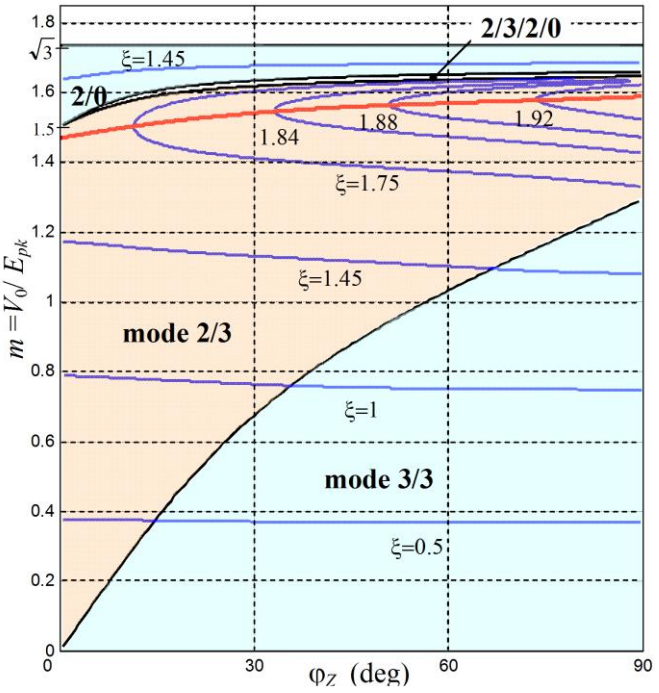

Fig. 6. Iso-ξ contour lines (blue) and MPPA trajectory (red) in the plane (φ_Z, m). In the operation at variable speed, φ_Z varies and the MPPA trajectory can be tracked by adjusting m, i.e. V_0.

Approximated expressions of m and ξ as a function of φ_Z for the MPPA operation are

$$m_{MPPA}(\varphi_Z) \cong 1.467 + 0.203\varphi_Z - 0.142\varphi_Z^2 + 0.0395\varphi_Z^3 \text{ , (17)}$$

$$\xi_{MPPA}(\varphi_Z) \cong 1.685 + 0.393\varphi_Z - 0.261\varphi_Z^2 + 0.076\varphi_Z^3 \text{ , (18)}$$

As shown in Fig. 5, the value of m for the MPPA is close to 1.5. Under a practical point of view, the MPPA operation for given parameters and for a given speed is achieved by a proper regulation of V_0 according to (17) and (4-a).

By considering the definition of ξ in (16), the expression of P_0^* as a function of φ_Z in the MPPA condition can be evaluated as the product of (18) times I_{rms}^*:

$$P_{0\,MPPA}^* = \xi_{MPPA}(\varphi_Z) I_{rms}^*(\theta_x, m_{MPPA}(\varphi_Z), \varphi_Z) \text{ . (19)}$$

By appending to (19) the constraint equation (8) with $m = m_{MPPA}$ (φ_Z), the variable θ_x can be eliminated. The following final approximated relation results:

$$P_{0MPPA}^*(\varphi_Z) \cong 0.137 - 0.146\varphi_Z + 0.085\varphi_Z^2 - 0.0052\varphi_Z^3 \text{ . (20)}$$

Finally, the expression of $I_{rms\,MPPA}^*(\varphi_Z)$ in the MPPA condition follows from (16), (18) and (20).

VI. Effect of the Eddy Currents

In high current machines, the stator winding conductors are composed by bars instead of thin wires. Thus, it is necessary to evaluate the eddy current losses which are also due to the significant harmonic content of the stator current. It is well known that the eddy losses due to the skin effect occur in the conductors even in the sinusoidal operation. They are taken into account by a factor k_R >1 which is used to increase the winding dc resistance to be used in the joule loss computation [25]. In sinusoidal operation, k_R essentially depends on the square of the frequency and on the 4th power of the thickness (normal to the slot leakage flux direction) of each single conductor. Moreover, k_R is affected by the division and transposition of the single conductors which form a slot conductor. As a result, the winding loss is given by

$$P_l = 3I_{rms}^2 k_R R = 3I_{rms}^2 (1 + (k_R - 1))R \text{ (21)}$$

In the last equality, the total ac resistance has been split into the dc component and the increment due to the skin effect.

If the winding current is distorted, as it happens in a PMSG connected to a diode rectifier, the global loss can be computed by adding the loss contribution due to the individual harmonics:

$$P_l = 3R\sum_k I_k^2 \left(1 + (k_R - 1)k^2\right) = 3I_{rms}^2 \tilde{k}_R R \text{ (22)}$$

where the new resistance factor $\tilde{k}_R$ is given by

$$\tilde{k}_R = 1 + (k_R - 1)\sum_k k^2 \frac{I_k^2}{I_{rms}^2} \text{ (23)}$$

Thus, $\tilde{k}_R$ depends on the harmonic content of the stator current, i.e. on the operation point of the rectifier in the plane (φ_Z, m). As a result, instead of the MPPA condition, which maximizes the ratio ξ (16), it is more interesting to consider the operation conditions which maximizes the ratio

$$\tilde{\xi} = \frac{P_0^*}{\sqrt{\tilde{k}_R} I_{rms}^*} = \frac{\xi}{\sqrt{\tilde{k}_R}} \text{ , (24)}$$

so that the Maximum Power per Effective Ampere (MPPEA) is achieved. When the skin effect is negligible (i.e. when k_R =1 so that also $\tilde{k}_R$ =1) $\tilde{\xi}$ reduces to ξ.

In (23)-(24) one can assume that the behavior of the rectifier is not deeply modified by the skin effect so that the expressions (7) and (10) can be still invoked. This is reasonable if the winding is designed in order to limit the factor k_R in such a way that (k_R −1) is few percent. This condition is also mandatory to limit the winding losses, as it will be shown later.

The analysis performed for ξ could be repeated also for $\tilde{\xi}$, namely: drawing the iso-$\tilde{\xi}$ lines in the plane and finding the MPPEA line. Intuitively, the MPPEA trajectory should belong between the MPPA and the MP lines. In fact, a slight decrease of m with respect to (17) (with fixed φ_Z) reduces ξ, but also

reduces the harmonic content of the current. As a consequence, the factor $\tilde{k}_R$ in the denominator in (24) decreases. For a small decrease of m with respect to (17), the reduction of $\tilde{k}_R$ is much more significant than the decrease of ξ, and the final effect is an increase of $\tilde{\xi}$.

An analytic study of $\tilde{\xi}$ would call for a preliminary evaluation of the amplitude of each current harmonic as a function of the operating parameters m and φ_Z. Unfortunately, these expressions are not available. Nevertheless, the optimal value of m which maximizes $\tilde{\xi}$ and the related value of $\tilde{k}_R$ have been found numerically for some values of φ_Z and k_R, by performing simulations in the time domain. To this purpose, the model of the ideal diode rectifier available in the Sim Power System library of Simulink has been used. Some results obtained with k_R=1.1 are collected in Table I. As a comparison, the value of ξ for the same angle φ_Z and m has been reported.

The results in Table I show that lower φ_Z results in higher eddy current losses due to the distorted current waveforms. Moreover, even by limiting the basic factor k_R to 1.1 by means of an appropriate division and transposition of the conductors in the slots, the contribution of eddy losses can be more than 25%, due to the distortion. Thus, with respect to the sinusoidal operation, a thinner division of each conductor is advisable in case of distorted waveforms.

TABLE.I. MPPEA CONDITION PARAMETERS FOR k_R=1.1.

φ_Z (rad)	π/6	π/4	π/3	5π/12	π/2
m_{MPPEA}	1.422	1.432	1.449	1.468	1.492
ξ	1.7574	1.7873	1.8201	1.8549	1.8977
$\tilde{\xi}_{MPPEA}$	1.5160	1.5664	1.6108	1.6559	1.7098
$\tilde{k}_R$	1.3438	1.3018	1.2767	1.2548	1.2320

VII. OPERATION TRAJECTORIES

Fig. 7 collects the most meaningful operation trajectories of a PMSG in the plane (φ_Z, m). For a full understanding of the operation features, such trajectories should be overlapped to the iso-P_0, iso-η and iso-ξ lines in Figs. 4-6.

If the PMSG works at variable speed and simultaneously the dc voltage is maintained constant, according to (2), (4)-(5), the angle φ_Z increases with the speed and the ratio m decreases. Thus the operating point of the PMSG follows trajectory (a). In spite of the progressive reduction of P_0^* for high speeds (see Fig. 4), the dimensional P_0 monotonically increases, due to the almost linear increase of the factor E_{pk}^2/Z in (9). Trajectory (a) also shows that if the speed is too low, the ratio m is higher than the minimum value required to make the diode bridge conducting (√3 for ideal diodes).

By contrast, if the PMSG operates at fixed speed and with variable dc voltage, the representative trajectory in the plane (φ_Z , m) is the vertical line (b), because the angle φ_Z is now constant. The movement along the vertical line is determined by a variation of m caused by the regulation of the dc voltage in (4-a), for instance by a dc-dc converter. Since in this last case the factor E_{pk}^2/Z is constant, Fig. 4 gives an immediate insight into the variation of the dimensional power P_0.

The other trajectories are the MP (c), MPPA (d) and MPPEA (e) lines, which have been already commented. The MPPEA trajectory (e) has been traced by interpolating the points in Table I. Even if the efficiency chart in Fig. 5 does not include the effect of the mechanical and iron losses, a comparison between Figs. 6 and 5 shows that in the operation in MP, the efficiency can be quite low, and the high losses, can produce overheating in the machine. The drop of the efficiency for low values of m is essentially due to the progressive phase displacement between the current and the EMF, whereas the THD of the stator current becomes lower and lower.

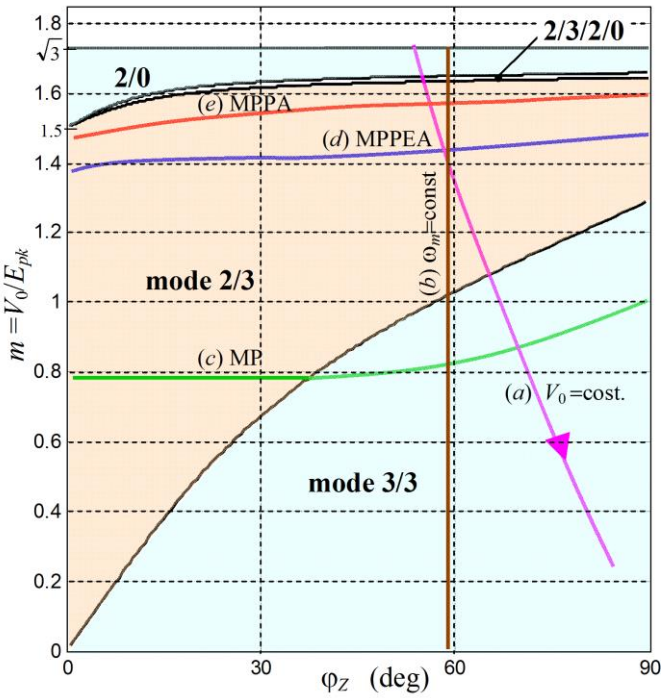

Fig. 7. Operation point trajectories. (a): constant V_0 and increasing ω_m. (b): constant speed ω_m and variable V_0. (c): MP, (d): MPPA, (e): MPPEA when k_R =1.1.

VIII. EXPERIMENTAL VALIDATION

Fig. 8 shows the experimental setup which has been used to validate the theoretical results. A dc motor drives the tested fractional slot surface mounted PMSG, a three-phase diode rectifier with a parallel R-C load is connected to the stator: the data of the PMSG and of the diodes are reported in the Appendix. A capacitor C_0 = 8.2 mF is designed to limit the ripple. The load is varied by adjusting the value of R_0 and, at the same time, the DC voltage V_0 is measured and used as independent variable in the description of the results. Several tests at different constant speeds have been performed. At first, the P_0 vs. V_0 and P_0/I_{rms} vs. V_0 theoretical curves are plotted by using the complete model [24] including the diode voltage

drops and they are compared to the experimental results. Then, the MP and MPPA points are extracted from the test results and are plotted as a function of φ_Z together with the simplified relations (12)-(13) and (17)-(20) in order to validate the theory developed in Sections III - IV.

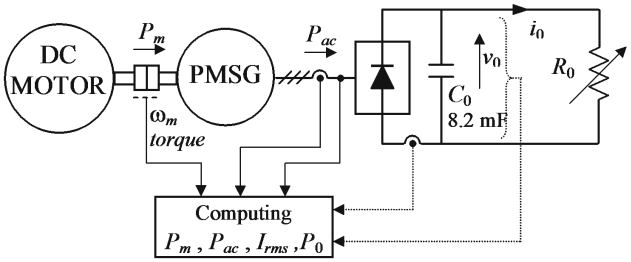

Fig. 8. Layout of the experimental setup

Fig. 9 shows the trend of the dc power P_0 versus the dc voltage V_0 for various values of the mechanical speed: the experimental points are close to the theoretical prediction (continuous line), and the maximum power is fairly predicted by the adopted model. No tests at the left of the MP points towards the short circuit condition have been performed: in fact, the operation in the range between the MP points and the short circuit would produce overheating of the PMSG and poor efficiency.

The trend of the p.u. ratio $\xi = P_0^*/I_{rms}^*$ versus the dc voltage V_0 is reported in Fig. 10 together with the experimental points: according to (15)-(16), experimental values of ξ are obtained by dividing the dimensional ratio P_0/I_{rms} by the EMF E_{pk} at each speed. Also in this case, the analytical model well predicts the trend of ξ as well as the localization and the value of its maxima. As the stator winding consists of thin wires (two 0.85 mm wires in parallel) the eddy current losses in the windings are negligible, so that $\tilde{\xi} \approx \xi$ can be assumed.

Fig. 11 reports the efficiency curves together with the experimental points. The mismatch is due to the presence of eddy currents in the solid rotor and PMs induced by the stator current harmonics, which have not been included in the model. Nevertheless, as expected, the abscissae of the MPPA and of the maximum efficiency points are very close. The analytical evaluation of the MPPA points allows to find the upper boundary of the range of V_0 the rated operation point should belong to.

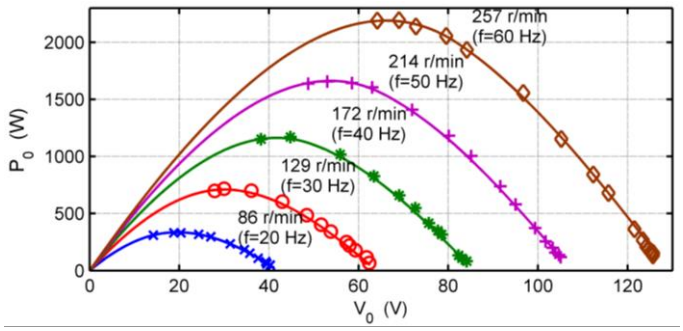

Fig. 9. Trend of P_0 versus V_0 for various constant speeds: continuous lines = theoretical model.

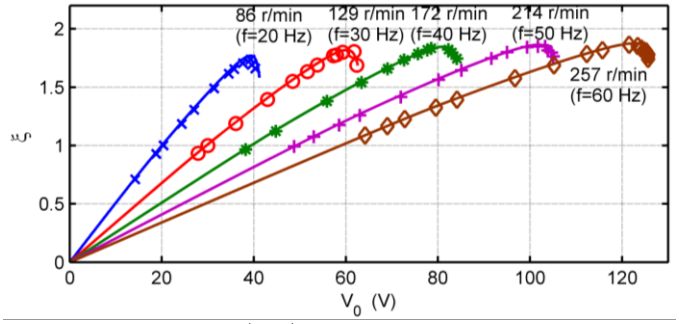

Fig. 10. Trend of $\xi=P_0^*/I_{rms}^*$ versus V_0 for various constant speeds: continuous lines = theoretical model.

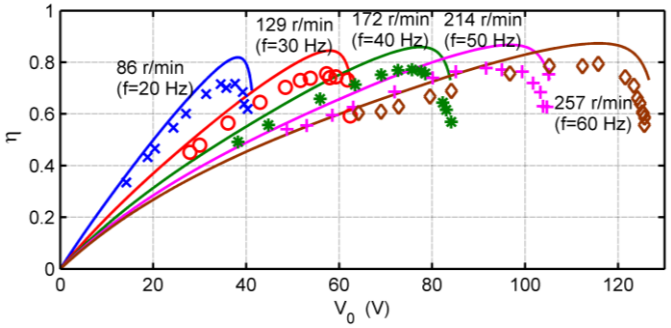

Fig. 11. Trend of the efficiency η versus V_0 for various constant speeds: continuous lines = theoretical model.

Fig. 12 shows the theoretical values of m_{MP} and m_{MPPA} provided by (12) and (17), respectively, whereas Fig. 13 reports the corresponding values of the p.u. dc power P_0^* given by (13) and (20): on the same figure, the experimental points are reported. The trend of ξ_{MPPA} (maximum achievable ξ) versus φ_Z (18) is shown in Fig. 14 together with the experimental points.

The analytical predictions are accurate: the maximum disagreement in the predictions of the maximum power $P_{0\,MP}^*$ and of the ratio ξ_{MPPA} by (13) and (18) occurs at low values of φ_Z (8% and 5% respectively). This is due to the fact that (12)-(20) are deduced by neglecting the threshold voltage drop V_D across diodes, whereas the theoretical curves in Fig. 10-12 take into account this effect by using a complete model [24]. It should be noticed that, in the performed tests, low values of φ_Z are obtained by driving the PMSG at low speed, which also implies low internal EMF E_{pk}. In these conditions, the diode threshold voltage V_D gives a small but noticeable contribution to the ratio m (4) and in the expression of P_0^* which is neglected in (12)-(20).

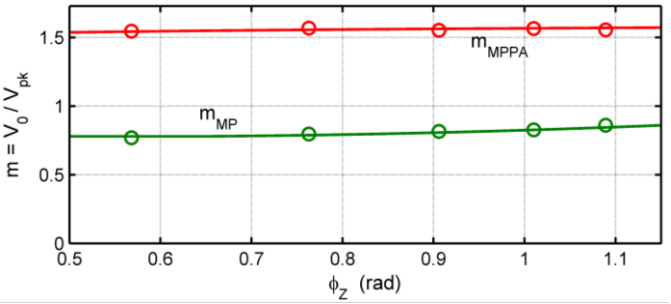

Fig. 12. Theoretical (by (12) and (17)) and experimental trends of $P_{0\,MP}^*$ and $P_{0\,MPPA}^*$ versus φ_Z.

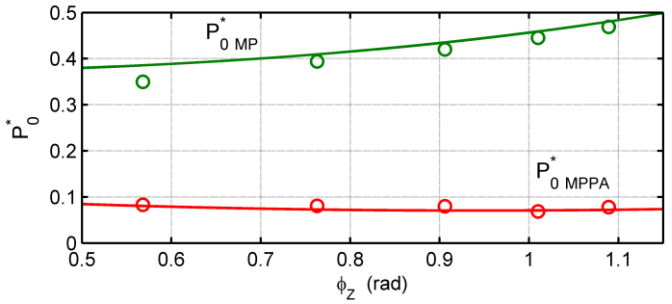

Fig. 13. Theoretical (by (13) and (20)) and experimental trends of $P_{0\,MP}{}^{*}$ and $P_{0\,MPPA}{}^{*}$ versus φ_Z.

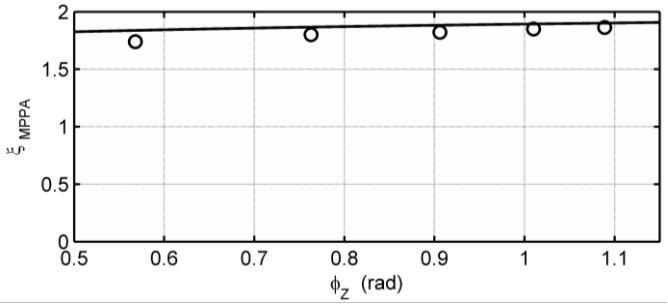

Fig. 14.Theoretical (18) and experimental trend of ξ_{MPPA} versus φ_Z.

These results prove that the analytical model developed in [24] and the relations deduced in Sections IV and V correctly predict the performances of a surface mounted PMSG also in the operation mode 2/3, which is the most interesting one for this kind of machines.

In order to appreciate the actual load level in the considered PMSG as well as the derating due to the diode bridge, Fig. 15 shows the p.u. dc power P_0/A_n versus the frequency along the MP and MPPA trajectories: to this purpose, the rated apparent power $A_n=\sqrt{3}V_nI_n$ of the PMSG is used as base value. Continuous lines depict the theoretical values calculated by the formulae deduced in Section IV and V, whereas circles depict the experimental results. Fig. 15 also reports the rated current limit of the stator which should not be overcome by the ac rms current: with the considered machine, the MP trajectory falls outside the area allowed by the thermal cooling. In particular, at the rated speed and frequency (50 Hz), the theoretical MP and MPPA are P_{0MP} = 0.87 p.u. and P_{0MPPA} = 0.135 p.u. respectively, whereas the maximum allowed dc power at the boundary of the current limit is 0.69 p.u.. The slight mismatch between the theoretical MP line and the experimental points is due to the effect of the diode bridge losses, which has been neglected in (12)-(20).

In the considered PMSG, the operation along the MPPA trajectory results in a low output power, namely in a low power density. However, the actual collocation of the current limit boundary between the MP and MPPA lines strongly depends on the design specifications of the PMSG. Under this point of view, the availability of (12)-(20) to predict the MP and MPPA conditions strongly helps the machine designer to optimize the PMSG size and the cooling system by favoring either power density or efficiency.

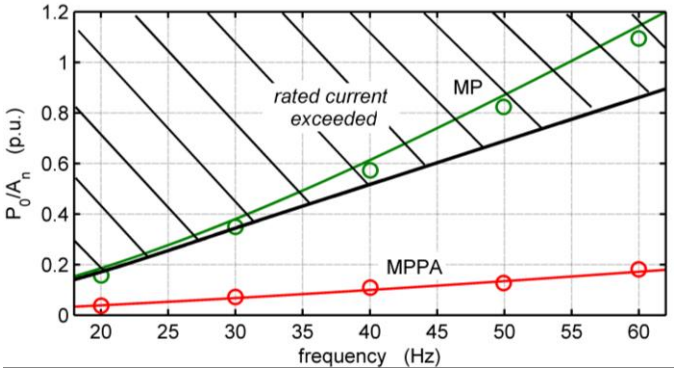

Fig. 15. p.u. delivered dc power P_0/A_n versus operation frequency along the MP and MPPA trajectories, and constraint due to the rated current limit.

Finally, Fig. 16 shows the theoretical MP and MPPA trajectories in the plane (ω_m/ω_{mn}, V_0) together with the experimental points. In practice, to trace Fig. 15, the dependence of φ_Z on ω given in (4)-(5) is inserted into (12) or (17) to express m_{MP} or m_{MPPA} as a function of ω or ω_m: after this, the values of m_{MP} or m_{MPPA} are converted into the dimensional voltage by using (4) and (2). These curves allow scheduling the appropriate value of V_0 as a function of the speed ω_m according to the desired control strategy.

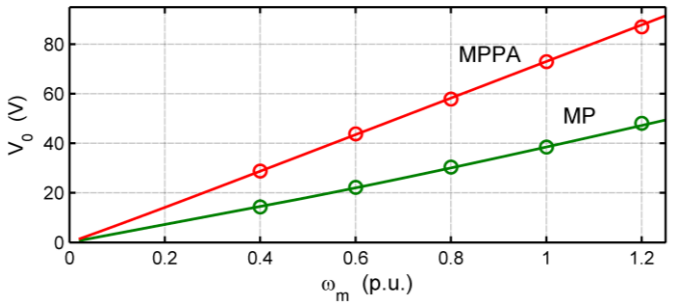

Fig. 16. Dc voltage versus normalized speed, required for the control along the MP and MPPA trajectories.

Note that all the trajectories investigated, and shown in Figs. 12-16, have also a useful design purpose: indeed, they can help the PMSG designer to properly choose the internal rated EMF amplitude, according to the design goal (i.e. maximizing the power or the power per ampere).

IX. Conclusion

The operation of a surface mounted PMSG connected to a diode rectifier with constant regulated dc voltage has been investigated in this paper. Such a system is currently used in low cost applications. Differently from some existing approaches, all the operation modes as well as the presence of the stator resistance are considered. The conditions for the maximum power transfer as well as for the maximum power per ampere have been stated analytically: they are represented by trajectories in the plane of internal impedance angle – normalized dc voltage. In general applications of the PMSG + diode bridge system, the compact analytical expressions deduced in this paper allow the PMSG designer to properly locate the rated operating point of the system within the zone characterized by high performance. Additionally, in the

particular case in which the PMSG can be controlled without regard for the optimization of the prime mover operation (as in small generators coupled to large engines and feeding ancillary services), the aforementioned trajectories allow the dc voltage to be scheduled to optimize the PMSG operation.

APPENDIX

PMSG data: V_n = 80.4 V (line to line), I_n = 14 A, ω_{mn}= 22.4 rad/s (214 r.p.m.), p=28 poles, R = 0.578 Ω, L = 3.15 mH, k_E = 0.148 V/(rad/s), c_0 = 0.317 Ws/rad, c_1 = 4.78 10^{-4} Ws^2/rad^2.

Diode data: V_D = 0.75 V, R_D = 42 mΩ (including the resistance of the connections).

ACKNOWLEDGMENT

Authors thank Valtaro Motori s.r.l., Borgo Val di Taro (PR) – Italy for providing magnetic laminations and mechanical parts for the prototype construction.

REFERENCES

[1] A. Grauers, " Efficiency of three wind energy generator systems," *IEEE Trans. En. Conv.*, vol. 11, no. 3, Sept. 1996, pp. 650-657.

[2] T. F. Chan, L.L. Lay, "Permanent magnet machines for distributed power generation: a review," *Proc. IEEE Power Eng. Soc. Gen. Meet.*, Jun. 2007, pp. 1-6.

[3] M. Chinchilla, S. Arnaltes, J. C. Burgos, "Control of permanent magnet generators applied to variable speed wind energy systems connected to the grid," *IEEE Trans. En. Conv.*, vol. 21, no. 1, Mar. 2006, pp. 130-135.

[4] M. Pathmanathan, W. L. Soong, N. Ertugrul, "Maximum-torque-per-ampere control of phase advance modulation of an SPM wind generator," *IEEE Trans. Ind. Appl.*, vol. 48, no. 5, Sept./Oct. 2012, pp. 1443-1451.

[5] K. Tan, S. Islam, "Optimal control strategies in energy conversion of PMSG wind turbine system without mechanical sensors," *IEEE Trans. En. Conv.*, vol. 19, no. 2, Jun. 2004, pp. 392-399.

[6] Md. Enamul Haque, M. Negnevitsky, K. M. Muttaqi, "A novel control strategy for a variable-speed wind turbine with a permanent-magnet synchronous generator," *IEEE Trans. Ind. Appl.*, vol. 46, no. 1, Jan. 2010, pp. 331-339.

[7] C. Xia, Q. Geng, X. Gu, T. Shi, Z. Song, "Input-output feedback linearization and speed control of a surface permanent-magnet synchronous wind generator with the boost-chopper converter," *IEEE Trans. Ind. Electron.*, vol. 59, no. 9, Sept. 2012, pp. 3489-3500.

[8] Xia, Y.Y., Fletcher, J.E., Finney, S.J., Ahmed, K.H., Williams B.W.: 'Torque ripple analysis and reduction for wind energy conversion systems using uncontrolled rectifier and boost converter', *IET Renew. Power Gener.*, 2011, 5, (5), pp. 377–386.

[9] A. Di Gerlando, G. Foglia, M. F. Iacchetti, R. Perini, "Analysis and Test of Diode Rectifiers Solutions in Grid Connected Wind Energy Conversion Systems Employing Modular Permanent Magnet Synchronous Generators," *IEEE Trans. Ind. Electron.*, vol. 59, no. 5, May 2012, pp. 2135-2146.

[10] J. Wang, D. Xu, Bin Wu, Z. Luo, "A low-cost rectifier topology for variable-speed high-power wind turbines," *IEEE Trans. Power Electron.*, vol. 26, no. 8, Aug. 2011, pp. 2192-2200.

[11] C. Xia, Z. Wang, T. Shi, Z. Song, "A novel cascaded boost chopper for the wind energy conversion system based on the permanent magnet synchronous generator," *IEEE Trans. En. Conv.*, vol. 28, no. 3, Sept. 2013, pp. 512-522.

[12] D. Oliveira, M. M. Reis, C. E. A. Silva, L. H. S. Colado Barreto, F. L. M. Antunes, B. L. Soares, "A three-phase high-frequency semi-controlled rectifier for PM WECS," *IEEE Trans. Power Electron.*, vol. 25, no. 3, Mar. 2010, pp. 677-685.

[13] A. Grauers, P. Kasinathan, "Force density limits in low-speed PM machines due to temperature and reactance," *IEEE Trans. En. Conv.*, vol. 19, no. 3, Sept. 2004, pp. 518-525.

[14] D.J. Perreault, V. Caliskan, "Automotive power generation and control," *IEEE Trans. Power Electron.*, vol. 19, no 3, pp. 618-630, May 2004.

[15] J. Rivas, D. Perreault, T. Keim, "Performance improvement of alternators with switched-mode rectifiers," *IEEE Trans. En. Conv.*, Vol. 19, No. 3, Sept. 2004.

[16] N. Patin, L. Vido, E. Monmasson, J. P. Louis, M. Gabsi, M. Lécrivain, "Control of a hybrid excitation synchronous generator for aircraft applications," *IEEE Trans. Ind. Electron.*, vol. 55, no. 10, 2008, pp. 3772-3783.

[17] W. U. N. Fernando, M. Barnes, O. Marjanovic, "Direct drive permanent magnet generator fed ac-dc active rectification and control for more-electric aircraft engines," *IET Elect. Power Appl.*, vol. 5, no. 1, Jan. 2011, pp. 14-27.

[18] J. Jatskevich, S. D. Pekarek, A. Davoudi, "Parametric average-value model of synchronous machine-rectifier systems," *IEEE Trans. En. Conv.*, vol. 21, no. 1, 2006, pp. 9-18.

[19] A. Cross, A. Baghramian, A. Forsyth, "Approximate, average, dynamic models of uncontrolled rectifiers for aircraft applications," *IET Pow. Electron*, vol. 2, no. 4, 2009, pp. 398-409.

[20] W.F. Ray, R.M. Davis, I.D., Weatherhogg "The three-phase bridge rectifier with a capacitive load," *IEE Conf. Publications*, London, UK, 1988, vol. 291, pp. 153–156.

[21] M. Hancock, "Rectifier action with constant load voltage: infinite capacitance condition," *Proc. Inst. Elect. Eng.*, London, UK, 1973, vol. 120, no. 12, pp. 1529–1530.

[22] V. Caliskan, D. J. Perreault, T. Jahns, J. G. Kassakian, "Analysis of three-phase rectifiers with constant-voltage loads", *IEEE Trans. Circuits Syst. I*, vol. 50, no. 9, 2003, pp. 1220, 1226.

[23] J. A. M. Bleijs, "Continuous conduction mode operation of three-phase diode bridge rectifier with constant load voltage," *IEE Proc. Electr. Power Appl.*, vol. 152, no. 2, 2005, pp. 359-368.

[24] A. Di Gerlando, G. M. Foglia, M. F. Iacchetti, R. Perini, "Comprehensive steady-state analytical model of a three-phase diode rectifier connected to a constant DC voltage source," *IET Power Electron.*. Vol. 6, no. 9, pp. 1927-1938, Nov. 2013.

[25] J. Pyrhonen, T. Jokinen, V. Hrabvocova, "Design of rotating electrical machines," John Wiley & Sons, 2008, pp. 259-261.

Matteo F. Iacchetti (M'10) received the Ph.D. degree in electrical engineering from the Politecnico di Milano, Milan, in 2008. From 2009 to 2014 he has been a post-doc researcher with the Dipartimento di Energia of the Politecnico di Milano, Milan, Italy. Currently, he is a Lecturer with the School of Electrical and Electronic Engineering at the University of Manchester, Manchester, UK. His main interests are design, modelling and control of electrical machines and electrical drives for power conversion.

Antonino Di Gerlando (M'93) received his MS degree in electrical engineering from the Politecnico di Milano, Italy, in 1981. Currently, he is a Full Professor at the Department of Energy at Politecnico di Milano. Fields of interest: design and modeling of electrical machines, converters and drive systems. He is a member of IEEE, of the Italian Association of the Electric and Electronic Engineers (AEI), of the Electric Italian Committee of Standards (CEI) and of the SC of ICEM Conference.

Giovanni Maria Foglia received his MS degree and the PhD in electrical engineering at Politecnico di Milano, Milano, Italy, in 1997 and 2000. Currently, he is an Assistant Professor at the Department of Energy at Politecnico di Milano, and his main field of interest is the analysis and design of PM electrical machines.

Andrew J. Forsyth (M'98–SM'07) received the B.Sc. (Eng.) degree from Imperial College, London, U.K., in 1981 and the Ph.D. degree from the University of Cambridge, Cambridge, U.K., in 1987. He was a Design Engineer with GEC Electrical Projects, Ltd., from 1981 to 1983, a Lecturer with the University of Bath, Bath, U.K., from 1986 to 1990, and a Lecturer/Senior Lecturer with the University of Birmingham, Birmingham, U.K., from 1991 to 2004. Since 2004, he has been a Professor of power electronics with the School of Electrical and Electronic Engineering, The University of Manchester, Manchester, U.K. His research interests include high-frequency converters, high-power factor rectifiers, modeling and control of autonomous power systems, and aerospace and electric-vehicle applications.